An atomistic-continuum hybrid simulation of fluid flows over superhydrophobic surfaces

Qiang Li and Guo-Wei He[a)]
*LNM, Institute of Mechanics, Chinese Academy of Sciences, Beijing 100080,
People's Republic of China*

Recent experiments have found that slip length could be as large as on the order of 1 μm for fluid flows over superhydrophobic surfaces. Superhydrophobic surfaces can be achieved by patterning roughness on hydrophobic surfaces. In the present paper, an atomistic-continuum hybrid approach is developed to simulate the Couette flows over superhydrophobic surfaces, in which a molecular dynamics simulation is used in a small region near the superhydrophobic surface where the continuum assumption is not valid and the Navier-Stokes equations are used in a large region for bulk flows where the continuum assumption does hold. These two descriptions are coupled using the dynamic coupling model in the overlap region to ensure momentum continuity. The hybrid simulation predicts a superhydrophobic state with large slip lengths, which cannot be obtained by molecular dynamics simulation alone. © *2009 American Institute of Physics.*
[DOI: 10.1063/1.3137674]

I. INTRODUCTION

Superhydrophobic surfaces, such as the lotus leaves, are extremely difficult to wet, with water contact angles in excess of 150°. The excessively big contact angles may induce a large slippage of liquid on superhydrophobic surfaces. It has many applications in reducing viscous drags and amplifying transport phenomena. For example, a boundary slip can enhance fluid flow in microdevices, where large surface effects resist fluid flow. Slippage can be measured by a slip length, the ratio of slip velocity to shear rate at the surfaces. Recent experimental studies and molecular dynamics (MD) simulations have reported a wide range of slip lengths from nanometers to micrometers. The typical slip lengths obtained from the experimental studies are tens of nanometers,[1–6] hundreds of nanometers,[7–11] and micrometers.[12–19] Recently, Lee *et al.* achieved giant slip lengths, as large as 185 μm.[20] They expected that the giant slip lengths could make a significant impact on high-Reynolds-number liquid flows, where the thickness of boundary layers is on the order of 1 mm. However, the MD simulations can only reach slip lengths up to hundreds of nanometers,[21–32] at least one order lower than the ones from the experimental studies. Due to computer power, the MD simulations to data are limited to tens of thousands of atoms. It restricts the space and time scales of the simulated physical systems. Therefore, the results from MD simulations are difficult in comparison with the experimental results. On the other hand, the Navier-Stokes (NS) equations are used to simulate the flows with slip boundaries at macroscales.[33–35] The imposed boundary conditions need to be justified to be consistent with superhydrophobicity.[36]

One solution to this problem is to use the atomistic-continuum hybrid simulation. In the hybrid simulation,[37] the fluid is simulated by MD simulations in a thin layer adjacent to the solid surfaces, where the continuum assumption breaks down, and the fluid in the domain for the bulk flows, described by the NS equations where the continuum assumption holds true. A constrained

---

a)Author to whom correspondence should be addressed. Electronic mail: hgw@lnm.imech.ac.cn.
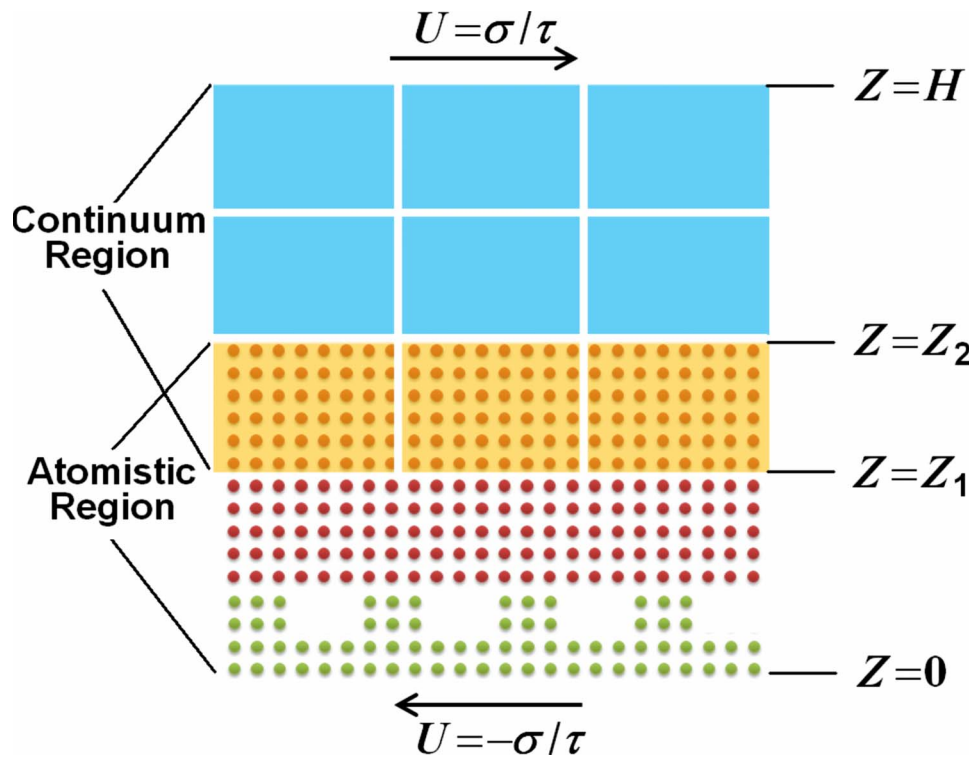
FIG. 1. The schematic plot for the Couette flow with the subdomains in the hybrid simulation. The region with meshes denotes the continuum region, while the region with dots denotes the atomistic region. The region with both meshes and dots denotes the overlap region.

particle dynamics[38–41] is used in the overlapping domain to extract the boundary conditions of the NS equations from the particle motions and transfer the macroscopic information of the NS equations to the particle motions. A dynamic coupling model[42] is usually used here to adjust the relaxation time scale. Since the MD in the hybrid simulation is only used for a small region, the hybrid simulation is feasible for the fluid slippage on superhydrophobic surfaces in the domain of microscales or larger.

The rest of the article is organized as follows: In Sec. II, we will give a brief introduction to the hybrid approach of NS equations and MD simulation. The implementation of the hybrid simulation will be presented in detail. In Sec. III, we will present the numerical results on flows over superhydrophobic surfaces. The superhydrophobic state is justified using the MD simulation. Finally, the conclusions and discussions will be provided in Sec. IV.

II. HYBRID COMPUTATIONS

In the hybrid approach, a computational domain is decomposed into three regions (see Fig. 1). A MD simulation is used in the atomistic region where the continuum assumption breaks down. The NS equations are used in the continuum region where the continuum assumption does hold. These two descriptions are coupled in the overlap region to exchange information between the MD simulation and the NS equations. For the Couette flows over a superhydrophobic surface, the bulk flows in the large portion of a computation domain are described by the NS equations, and the small region near the superhydrophobic surface is described by the MD simulations. A constrained particle dynamics is constructed in the overlap region to ensure the momentum continuity between the continuum and atomic regions. Therefore, the hybrid simulation can save huge computational cost and is affordable for such type of micro- and nanofluidics as fluid flows over superhydrophobic surfaces. The results from a MD simulation on a small domain cannot be simply extended to

a large domain since the slip length is related to the shear rate, which is dependent on the domain size. The nonlinear velocity profile near superhydrophobic surfaces makes it more difficult to extend the results in a small domain to the ones in a large domain.

In the continuum region, the fluid flows are described by the NS equations:

$$\nabla \mathbf{u} = \mathbf{0}, \tag{1}$$

$$\rho \frac{\partial \mathbf{u}}{\partial t} + \rho \mathbf{u} \nabla \mathbf{u} = -\nabla p + \mu \nabla^2 \mathbf{u}, \tag{2}$$

where $\mathbf{u}$ is the fluid velocity, p is the pressure, ρ is the constant density, and μ is the viscosity. The NS equations are numerically solved by the explicit projection method on staggered grids. The pressures are defined at the center of a cell, and the velocities defined at the middle of cell sides. The time step Δt_{FD} for numerical integration should be smaller than the characteristic time of the flows: $\Delta t_{FD} \ll \rho \Delta x \Delta z / \mu$.

In the atomistic region, fluids are represented by an amount of particles whose ensemble averages give the macroscopic states. The interactions between the particles are described by a modified Lennard-Jones (LJ) potential:

$$V_{ij}(r) = 4\epsilon_{ij} \left[\left(\frac{\sigma_{ij}}{r} \right)^{12} - c_{ij} \left(\frac{\sigma_{ij}}{r} \right)^6 \right], \tag{3}$$

where ϵ_{ij} and σ_{ij} are the characteristic energy and length scales, respectively. The surface energy is adjusted by the coefficients c_{ij}, where the indices $i,j=f,s$ refer to the fluid or solid phase. The equation of motion for atoms is

$$m_i \frac{d^2 \mathbf{r}_i}{dt^2} = -\sum_{j \neq i} \frac{\partial V_{ij}}{\partial \mathbf{r}_i} \equiv \mathbf{F}_i. \tag{4}$$

Here, each particle has the mass m and the mass density is $\rho = 0.75 m \sigma^{-3}$. The equation of motion is integrated using the Verlet scheme, which yields

$$\mathbf{r}_i(t + \triangle t_{MD}) = 2\mathbf{r}_i(t) - \mathbf{r}_i(t - \triangle t_{MD}) + \triangle t_{MD}^2 \mathbf{F}_i / m, \tag{5}$$

$$\mathbf{v}_i(t) = \frac{\mathbf{r}_i(t + \triangle t_{MD}) - \mathbf{r}_i(t - \triangle t_{MD})}{2 \triangle t_{MD}}, \tag{6}$$

where $\mathbf{r}_i$ denotes the position of the ith particle, $\mathbf{v}_i$ is the velocity of the ith particle, and $\mathbf{F}_i$ is the force acting on the ith particle by all other particles. The time step is $\Delta t_{MD} = 0.005\tau$, in which $\tau = \sqrt{m\sigma^2}$ is the characteristic time of the LJ potential. These quantities will be nondimensionalized using the parameters m, σ, τ, and ϵ.

A Langevin thermostat is used to maintain a constant temperature T. This can be achieved by adding a Langevin noise and a frictional force to the equations of motion,

$$m \frac{d^2 \mathbf{r}_i}{dt^2} = \mathbf{F}_i - m\Gamma \frac{d\mathbf{r}_i}{dt} + \boldsymbol{\eta}_i, \tag{7}$$

where Γ is a friction constant that controls the rate of exchange with the thermostat. $\boldsymbol{\eta}_i$ is the Gaussian random force of the zero mean and the variance being $2mk_B T\Gamma$. (k_B is the Boltzmann constant.) The thermostat is kept on the homogeneous plane with the rate $\Gamma = \tau^{-1}$.

To ensure the momentum continuity in the overlap region, a constrained particle dynamics is introduced,

$$\frac{d^2\mathbf{r}_i}{dt^2} = \mathbf{F}_i + \xi\left(\mathbf{u}_J - \frac{1}{N_J}\sum_{j=1}^{N_J}\frac{d\mathbf{r}_j}{dt}\right),$$ (8)

where $\mathbf{u}_J$ is the fluid velocity in the Jth cell and N_J is the number of particles in the Jth cell. ξ is a coupling parameter, which makes the momentum consistent between the atomistic and continuum descriptions. This requires that the local averages of particle momenta have to be equal to the instantaneous macroscopic momentum. The requirement yields

$$\xi_J(t + \Delta t) = \frac{\frac{1}{N_J}\sum_{i=1}^{N_J}\left(\frac{d^2r_i(t)}{dt^2} - \frac{F_i(t)}{m}\right)}{u_J(t) - \frac{1}{N_J}\sum_{j=1}^{N_J}v_j(t)}.$$ (9)

The coupling parameter is determined by the current states in each cell at every time step. It adjusts the particle dynamics themselves as the computation progresses. Therefore, it controls the relaxation rate of the local mean of the particle momenta to the macroscopic momentum.

The hybrid approach using dynamic coupling model was tested against the sudden-started Couette flows with nonslip and slip boundary conditions. The results obtained are in good agreement with the results from a full MD simulation.[42] Furthermore, the hybrid approach is used to simulate the Couette flows with an oscillatory upper plate.[42] The results obtained are also in agreement with the ones from a full MD simulation. Those test cases validate the dynamic coupling model. In the hybrid approach, the dynamic coupling model for momentum continuity is shown to be numerically stable, while the coupling model for flux continuity is numerically unstable.[43]

III. NUMERICAL RESULTS

We will simulate a Couette flow over a superhydrophobic surface using the hybrid method of the NS equations and MD simulation. The Couette flow is the viscous fluids confined between two parallel plates, where the upper and lower plates are moved at equal and opposite speeds $\pm U = \pm \sigma/\tau$. A periodic boundary condition is applied in the streamwise direction. The channel height H between its two plates is 3060.5σ, and the channel width between its inlet and outlet is 341.5σ. A superhydrophobic surface is imposed onto the lower plate. Obviously, the Couette flow over a superhydrophobic surface cannot be simulated by either the NS equations or MD simulation alone.

To check the superhydrophobicity of the lower plate, a full MD simulation will be used to simulate fluid droplets on both hydrophobic and superhydrophobic surfaces in an affordable domain. The contact angles obtained will be compared with theoretical estimations. A superhydrophobic surface can be achieved by the combination of surface morphology and surface hydrophobicity. Here, the roughness of height 3.14σ and width 2.10σ are periodically placed on the surface at a distance 17.47σ. In the present simulation, all interactions between atoms are of the LJ type: the parameters for solid atoms are taken as $\epsilon_s=1.5$, $\sigma_s=1.0$, and $c_{ss}=1.0$; the parameters for fluid atoms are taken as $\epsilon_f=1.5$, $\sigma_f=1.0$, and $c_{ff}=1.0$; the parameters for the interactions between fluid and solid atoms are $\epsilon_{fs}=1.5$, $\sigma_{fs}=1.0$, and $c_{fs}=0.5$. Those parameters for the intermolecular attraction lead to a hydrophobic surface.

The continuum region is divided into 30×300 grids in the streamwise and vertical directions, respectively, while periodic boundary conditions are applied in the streamwise direction. A standard second-order central-difference scheme on a staggered grid is used, with the pressure and scalar variables located at the center of the grid cell and velocity components located at the cell face centers. The explicit projection method is used to integrate the NS equations. The simulation is conducted at $\text{Re}=UL/\nu=38.75$, where U and L, respectively, denote the velocity of the plate and the vertical length of the continuum region. We use $\triangle t_{\text{FD}}=50\triangle t_{\text{MD}}=0.25\tau$, which is smaller than the characteristic time of the flows and big enough to ensure the evolution of the MD simulations.
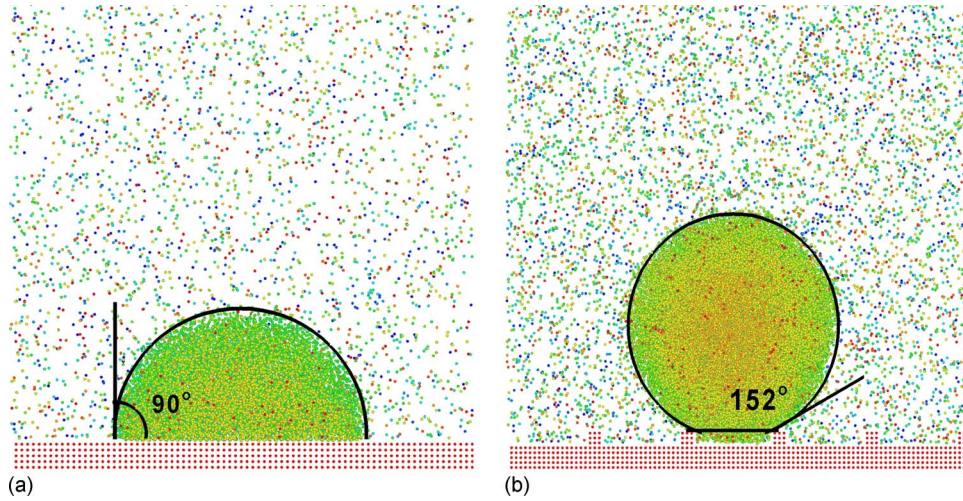
FIG. 2. Molecular configurations of liquid droplets on solid surfaces (side view): (a) The droplet on a flat and hydrophobic surface has the contact angle of 90°; (b) the droplet on a superhydrophobic surface has the contact angle of 152°. The superhydrophobic surface in (b) is made by patterning periodic roughness on the hydrophobic surface in (a). The molecules are marked by different colors for visualization.

The MD simulations are performed using the powerful code LAMMPS.[44] The atoms are initially placed on the face-centered-cubic (fcc) lattices. As the upper plate moves up, those atoms accumulate on a droplet on the surface. As soon as the droplet achieves a steady state, the upper plate stops moving. The periodic boundary conditions are taken in both the horizontal and spanwise directions. Figure 2 shows the atom configurations of droplets on the hydrophobic and superhydrophobic surfaces. The interactions between solid and fluid atoms are exactly the same in those two cases. However, the surface in Fig. 2(a) is flat and the one in Fig. 2(b) is patterned by the periodic roughness as described before. In Fig. 2(a), the simulated region is $69.01\sigma \times 69.01\sigma \times 108.32\sigma$ and the number of atoms is 48 810. In Fig. 2(b), the simulated region is $69.01\sigma \times 69.01\sigma \times 99.59\sigma$ and the number of atoms is 50 250. The same domain size and atom number as the ones in Fig. 2(a) are also used in the case of superhydrophobic surfaces. It also yields a superhydrophobic state with the droplet off the domain center. For visualization purposes, we plot the present figure. The droplets formed on the surfaces are used to calculate the contact angles using a circle fitting method. It gives the contact angle of 90° in Fig. 1(a) and the contact angle of 152° in Fig. 1(b). The contact angle on the flat surface can be also analytically calculated using the formula $\cos\theta = -1 + 2(\rho_s c_{fs})/(\rho_f c_{ff})$. The result is $\theta = 90°$, which is in agreement with the measurement from the MD simulations.

Next, we will use the hybrid approach to simulate the Couette flows over a superhydrophobic surface in a larger domain. In the hybrid method, the computational domain $0 \leq z \leq 3060.5\sigma$ is divided into two regions (see Fig. 1): the upper one at $z_1 \leq z \leq H$ ($z_1 = 60.5\sigma$) is described by the NS equations, and the lower one at $0 \leq z \leq z_2$ ($z_2 = 86.0\sigma$) is described by MD. The overlap region at $z_1 \leq z \leq z_2$ is described by the constrained particle dynamics. The boundary condition of the NS equations at z_1 is obtained from locally averaging the velocities of the particles in each cell of the overlap region. The constrained forces are added to the particles in the overlap region, according to the constrained particle dynamics, to convey the information from the NS equations to the MD simulations. The overlap region has three cells in the z direction. A constrained layer consists of the cells closest to the interface between the continuum and the atomistic regions. The constrained layer is used at $z = z_2$ to prevent the particles from spreading freely away from the MD region. The boundary condition at $z = 0$ is simulated by two (111) layers of a fcc lattice consisting of solid particles with the same mass and density as the fluid. Those particles are fixed in the MD simulations and interact with fluid particles in terms of a modified LJ potential. The MD simulations are carried out at a consistent temperature $T = 1.1\epsilon/k_B$. The velocity component in the direction
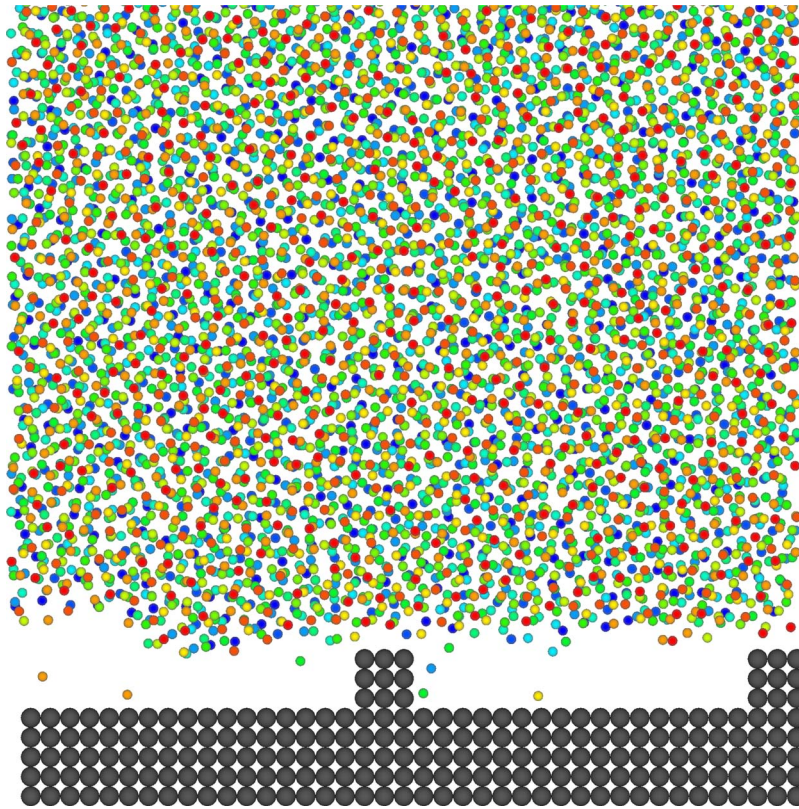
FIG. 3. The atom configuration of fluid in the Couette flow near the lower plate. The space between the roughnesses is essentially free from fluid atoms. The hybrid simulation predicts a superhydrophobic state on the lower plate.

orthogonal to the flow is thermostatted in order to avoid viscous heating in the fluid slab. We first run the MD for an equilibrium state. Then the MD and the NS equations are solved simultaneously for $20\,000\tau$ to achieve a steady state.

Figure 3 shows the side view of the atom configuration of the fluid flows near the superhydrophobic surface. There are very few atoms inside the rooms near the roughness. In other words, the cavities are essentially free from the atoms. This suggests a superhydrophobic state.

Figure 4 shows the steady solution of the Couette flow, whose lower plate is the same superhydrophobic surface as the one shown in Fig. 1(b). In the overlap region, an excellent agreement of the velocity profiles obtained from the NS equations and the MD simulation is observed, which demonstrates that the dynamic model correctly describes the momentum coupling between the atomistic and continuum dynamics. A thin layer is found near the solid-fluid interface, where velocity decreases slowly. This suggests a rapid decrease in viscosity predicted by Vinogradova,[45] which leads to a connection between atomistic slip and effective slip felt by fluid flows. A large slip velocity of $0.3\sigma/\tau$ is found near the superhydrophobic surface, with the effective slip length $\delta \sim 800\sigma$. Here, we use the effective slip length to make the measurement.[46] To our knowledge, this may be the largest slip length that the current numerical simulations can achieve for linear shear rates.

IV. DISCUSSION AND CONCLUSIONS

The slippage of liquids on superhydrophobic surfaces has been achieved by many experimental studies. However, the large slip lengths at microscales cannot be achieved by the MD simulations due to computer capability. The present work develops a hybrid approach of the NS equations and MD to simulate the Couette flows over superhydrophobic surfaces in a large domain,
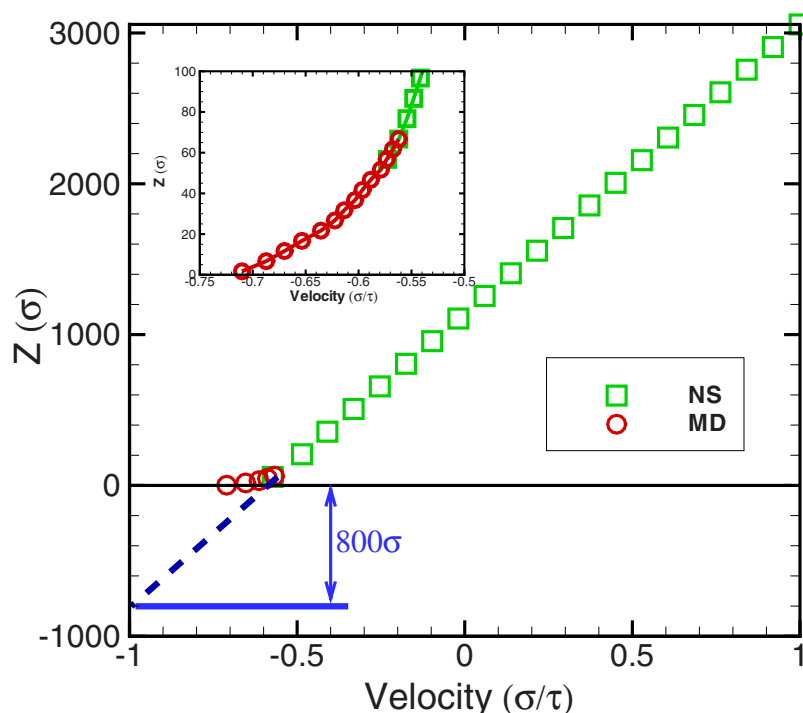
FIG. 4. The steady state of the velocity profile of a Couette flow over a superhydrophobic plate. Green squares denote the portion of the velocity profile obtained from the NS equations and red circles denote the one obtained from MD simulation. The inset shows the enlarged portion of the velocity profile near the superhydrophobic surface.

which cannot be simulated by the MD alone. A dynamic coupling model is used to eliminate the free parameters and give the correct relaxation time scales. The hybrid approach with a dynamic coupling model has been validated against a full MD simulation for the Couette flows with slip and nonslip boundary conditions at nanoscales. By the carefully chosen parameters in the LJ potentials, our numerical results achieved a large slip length of 800σ or 272 nm for argon. To our knowledge, the slip length is larger than any other ones obtained from the current numerical simulations. Our results suggest that slip lengths are dependent on the properties of both the LJ fluids and the material surfaces. Therefore, superhydrophobicity may become a new way to control fluid flows at nano- and microscales. The hybrid simulation provides an alternative, in addition to experiments, to explore and design superhydrophobic surfaces.

ACKNOWLEDGMENTS

[1] V. S. Craig, C. Neto, and D. R. Williams, Phys. Rev. Lett. **87**, 054504 (2001).
[2] C. H. Choi, K. J. A. Westin, and K. S. Breuer, Phys. Fluids **15**, 2897 (2003).
[3] S. Jin, P. Huang, J. Park, J. Y. Yoo, and K. S. Breuer, Exp. Fluids **37**, 825 (2004).
[4] C. Cottin-Bizonne, B. Cross, A. Steinberger, and E. Charlaix, Phys. Rev. Lett. **94**, 056102 (2005).
[5] B. Cross, A. Steinberger, C. Cottin-Bizonne, J. P. Rieu, and E. Charlaix, Europhys. Lett. **73**, 390 (2006).
[6] C. D. Honig and W. A. Ducker, Phys. Rev. Lett. **98**, 028305 (2007).
[7] R. Pit, H. Hervet, and L. Leger, Tribol. Lett. **7**, 147 (1999).
[8] C. Neto, V. S. J. Craig, and D. R. M. Williams, Eur. Phys. J. E **12**, 71 (2003).
[9] T. Schmatko, H. Hervet, and L. Leger, Phys. Rev. Lett. **94**, 244501 (2005).
[10] P. Huang, J. S. Guasto, and K. S. Breuer, J. Fluid Mech. **566**, 447 (2006).
[11] P. Huang and K. S. Breuer, Phys. Fluids **19**, 028104 (2007).
[12] Y. X. Zhu and S. Granick, Phys. Rev. Lett. **87**, 096105 (2001).

[13] J. Ou, B. Perot, and J. P. Rothstein, Phys. Fluids **16**, 4635 (2004).

[14] J. Ou and J. P. Rothstein, Phys. Fluids **17**, 103606 (2005).

[15] M. Majumder, N. Chopra, R. Andrews, and B. J. Hinds, Nature (London) **438**, 44 (2005); **438**, 930(E) (2005).

[16] C.-H. Choi, U. Ulmanella, J. Kim, C.-M. Ho, and C.-J. Kim, Phys. Fluids **18**, 087105 (2006).

[17] C.-H. Choi and C.-J. Kim, Phys. Rev. Lett. **96**, 066001 (2006).

[18] P. Joseph, C. Conttin-Bizonne, J. M. Benoît, C. Ybert, C. Journet, P. Tabeling, and L. Bocquet, Phys. Rev. Lett. **97**, 156104 (2006).

[19] R. Truesdell, A. Mammoli, P. Vorobieff, F. van Swol, and C. J. Brinker, Phys. Rev. Lett. **97**, 044504 (2006).

[20] C. Lee, C.-H. Choi, and C.-J. Kim, Phys. Rev. Lett. **101**, 064501 (2008).

[21] P. A. Thompson and M. O. Robbins, Phys. Rev. A **41**, 6830 (1990).

[22] D. L. Morris, L. Hannon, and A. L. Garcia, Phys. Rev. A **46**, 5279 (1992).

[23] P. A. Thompson and S. M. Troian, Nature (London) **389**, 360 (1997).

[24] J. L. Barrat and L. Bocquet, Faraday Discuss. **112**, 119 (1999).

[25] J. L. Barrat and L. Bocquet, Phys. Rev. Lett. **82**, 4671 (1999).

[26] A. Jabbarzadeh, J. D. Atkinson, and R. I. Tanner, Phys. Rev. E **61**, 690 (2000).

[27] M. Cieplak, J. Koplik, and J. R. Banavar, Phys. Rev. Lett. **86**, 803 (2001).

[28] T. M. Galea and P. Attard, Langmuir **20**, 3477 (2004).

[29] J. H. Walther, T. Werder, and R. L. Jaffe, Phys. Rev. E **69**, 062201 (2004).

[30] N. V. Priezjev, A. A. Darhuber, and S. M. Troian, Phys. Rev. E **71**, 041608 (2005).

[31] B. Y. Cao, M. Chen, and Z. Y. Guo, Phys. Rev. E **74**, 066311 (2006).

[32] M. Cieplak, J. Koplik, and J. R. Banavar, Phys. Rev. Lett. **96**, 114502 (2006).

[33] T. Min and J. Kim, Phys. Fluids **16**, L55 (2004).

[34] D. You and P. Moin, Phys. Fluids **19**, 081701 (2007).

[35] M. B. Martell, J. B. Perot, and J. P. Rothstein, J. Fluid Mech. **620**, 31 (2009).

[36] H. Brenner and V. Ganesan, Phys. Rev. E **61**, 6879 (2000).

[37] N. G. Hadjiconstantinou and A. T. Patera, Int. J. Mod. Phys. C **8**, 967 (1997).

[38] S. T. O'Connell and P. A. Thompson, Phys. Rev. E **52**, R5792 (1995).

[39] E. G. Flekkoy, G. Wagner, and G. Feder, Europhys. Lett. **52**, 271 (2000).

[40] X. B. Nie, S. Y. Chen, W. N. E, and M. O. Robbins, J. Fluid Mech. **500**, 55 (2004).

[41] J. Cui, G.-W. He, and D. W. Qi, Acta Mech. Sin. **22**, 503 (2006).

[42] Y.-C. Wang and G.-W. He, Chem. Eng. Sci. **62**, 3574 (2007).

[43] W. Q. Ren, J. Comput. Phys. **227**, 1353 (2007).

[44] We have used the MD code by S. Plimpton, computer code LAMMPS, 2008, which is available at http://lammps.sandia.gov/.

[45] O. I. Vinogradova, Langmuir **11**, 2213 (1995).

[46] E. Lauga and H. A. Stone, J. Fluid Mech. **489**, 55 (2003).